Correlation-based double-directional stochastic channel model for multiple-antenna ultra-wideband systems

X. Hong, C.-X. Wang, B. Allen and W.Q. Malik

Abstract: A correlation-based double-directional stochastic channel model for indoor multiple-input multiple-output (MIMO) ultra-wideband (UWB) propagation channels is proposed. The proposed model extends the IEEE 802.15.3a standard model to spatially correlated MIMO channels. Both angular and temporal statistics are taken into account in the modelling procedure. Spatial correlation is introduced into the multipath amplitude and time-of-arrival (ToA) matrices of the channel model. Each amplitude matrix consists of entries of correlated lognormal random variables, whereas each ToA matrix is obtained as the sum of a reference matrix and a difference matrix. The frequency-dependent spatial correlation function is derived to give an insight of model properties. Model parameters are determined based on well-known measurement campaigns. In addition, simulation-based analysis indicates that this model has desirable spatial correlation properties in both the time and frequency domains. The ToA correlation matrix was also found to have dominant effects on the correlation characteristics. This suggests that future research into spatial correlation properties of MIMO-UWB channels should focus on ToA correlation characteristics, rather than amplitude correlation characteristics, which are the current focus of narrowband and wideband MIMO channel research.

1 Introduction

Ultra-wideband (UWB) wireless systems have attracted great interest in both industry and academia during the past few years. By definition, UWB systems are severely limited in the transmit power but have very large bandwidth. Compared with conventional narrowband systems, UWB communication systems show a number of important advantages such as resistance to fading, high capacity, low power consumption and potentially low cost. As a result, UWB is widely envisioned as a universal technology for short range communications and sensor networks [1].

However, UWB's competitiveness is diminishing with advances in competing high data rate technologies, such as high speed packet access [2] and millimeter wave communications [3]. Multiple-input multiple-output (MIMO) is a promising technique that can be used to enhance UWB systems to extend the coverage, increase the robustness of the link and offer multi-gigabit rates [4–9]. A MIMO-UWB system deploys multiple antennas at both ends of the communication link and can be leveraged to provide array gain, diversity gain and multiplexing gain or a combination of all these. Array gain increases the signal-to-noise ratio valuable to power-constrained UWB systems and can be achieved by beamforming [4]. A 5.9 dB array gain, for instance, can compensate for transmission loss through a brick wall [1, pp. 280] or extend the coverage to approximately two times in an open space [5]. Diversity gain can either improve link robustness or extend coverage [5–7], whereas multiplexing gain can extend the UWB data rate to multiple gigabits [5, 8, 9]. There are trade-offs among the above gains [10] and one can be sacrificed for another depending on the requirements. Besides these well known gains, MIMO-UWB holds other promises such as interference cancellation [11], immunity against timing jitter [12] and reducing the complexity of Rake receivers [13, 14]. Furthermore, single-antenna UWB systems can cooperatively form a virtual MIMO system that can especially be useful for energy-constrained sensor devices.

Appropriate characterisation and modelling of MIMO-UWB propagation channels is indispensable for the design and performance evaluation of these systems. The current IEEE 802.15.3a and 802.15.4a channel models, however, do not support MIMO-UWB channels [15]. The unrealistic assumption of spatially uncorrelated channels will convert a MIMO-UWB channel into independent single-input-single-output (SISO) channels [15]. Because of its simplicity, this assumption has been applied to evaluate the performance of MIMO-UWB systems in [6, 7, 16]. However, since realistic MIMO-UWB channels are in general spatially correlated [17], such an assumption will lead to positively biased estimates of the system performance [18]. Moreover, the assumption of uncorrelated channels gives no guideline for antenna deployment in a practical system, such as

doi:10.1049/iet-map:20060223

Paper first received 1st September 2006 and in revised form 31st July 2007

X. Hong and C.-X. Wang are with School of Engineering and Physical Sciences, Electrical, Electronic and Computer Engineering, Joint Research Institute of Signal and Image Processing, Heriot-Watt University, Edinburgh EH14 4AS, UK

B. Allen is with the Department of Engineering Science, University of Oxford, Parks Road, Oxford OX1 3PJ, UK

W.Q. Malik is with the Laboratory for Information and Decision Systems, Massachusetts Institute of Technology, 77 Massachusetts Avenue, Cambridge, MA 02139, USA

E-mail: xh12@hw.ac.uk

spacing requirements of antenna arrays. Therefore it is of fundamental importance to theoretically analyse and simulate the spatial correlation properties of MIMO-UWB channels. This will enable us to study the impact of spatial correlation on the performance of MIMO-UWB systems and to derive realistic performance bounds.

To the best of the authors' knowledge, there are only a few MIMO-UWB channel models presented in the literature. A geometrically-based stochastic model [19] for space-variant UWB channels was presented in [20, 21] and a simple parametric stochastic model (PSM) [19] was introduced in [22]. A major drawback of these two models is that it is difficult to integrate them into a theoretical framework. This is largely because of the fact that they have implicit spatial correlation characteristics. Consequently, they provide little insight into the capacity and signalling design for a realistic MIMO-UWB system. From the information-theoretic and signal processing perspective, it is more desirable to have a correlation-based stochastic model (CBSM) [19] that can address explicitly the spatial correlation characteristics of MIMO-UWB channels. In [12], a CBSM adopting the tapped-delay-line structure was presented and the UWB channel coefficients were characterised as real Gaussian random variables (RVs). The accuracy of such a model is poor since the clustering effects [15], typically observed in UWB channels, were not taken into account. An improved CBSM was proposed in [23] based on the IEEE 802.15.3a standard SISO-UWB model [15]. The IEEE 802.15.3a model describes the UWB channel as a discrete sum of multipath components (MPCs), each characterised by its real-valued amplitude and time-of-arrival (ToA). Note that this approach differs from traditional narrowband/wideband channel modelling where MPCs are characterised by complex RVs. In [23], the multipath amplitudes from different antennas were considered as spatially correlated, whereas the ToAs were assumed to be spatially identical. This assumption in [23] implies that the correlation properties of MIMO-UWB channels can largely be represented by the spatial correlation of multipath amplitudes in the sub-channels, whereas the differences of ToAs can be neglected. This assumption is intuitively incorrect, since the high time resolution of UWB signals will result in ToA differences even between closely-spaced array elements.

In this paper, we propose a MIMO-UWB channel model which combines the advantages of both CBSM and PSM approaches. On one hand, the proposed model adopts the tapped-delay-line structure and incorporates angle-of-arrival (AoA) and angle-of-departure (AoD) double directional characteristics, as in a PSM [24]. On the other hand, the model deploys a correlation-based structure to provide explicit expressions of the spatial correlation properties of a MIMO-UWB channel, as in a CBSM [25]. Different from [23], the proposed model takes into account the spatial variations of not only multipath amplitudes but also ToAs. For each MPC, an amplitude correlation matrix and a ToA correlation matrix are defined separately. Such a modification is not trivial since the ToA correlation is shown to be crucial in obtaining frequency-dependent correlation properties, which is typical for MIMO-UWB channels [26–28]. Simulation results demonstrate that the correlation characteristics of our model match experimental observations [9, 26–29] in both the time and frequency domains. Also, the proposed model is consistent with the IEEE 802.15.3a model [15] and extends it from SISO to MIMO systems.

The rest of the paper is organised as follows. A double-directional SISO-UWB spatial channel model (SCM) is introduced in Section 2. In Section 3, we propose a correlation-based double-directional MIMO-UWB channel model and analyse its spatial correlation properties. Section 4 evaluates the proposed model based on simulation results and discusses their implications. Finally, conclusions are drawn in Section 5.

2 A double-directional SISO-UWB channel model

2.1 A double-directional Saleh–Valenzuela (S–V) model

The IEEE 802.15.3a group proposed a standard SISO-UWB channel model [15] derived from the S–V model [30] with some modifications. The S–V model describes the multipath clustering effects typically observed in indoor channels. It expresses the channel impulse response as a collection of clusters, where each cluster is itself a collection of several closely arriving rays. The clusters are determined by the macro layout of scatterers such as the ceiling, furniture and people, while the rays are formed as a result of the micro attributes of scatterers such as their shapes. In the case of UWB, because of its large bandwidth and fine time resolution, different parts of the same object can give rise to several rays, all of which would be part of a cluster.

One drawback of the IEEE 802.15.3a model is that it does not consider the directional properties of the channel. Thus, this model cannot be directly extended to MIMO-UWB channels. Our first task is therefore to incorporate directional characteristics [24] into the IEEE 802.15.3a model, resulting in SISO-UWB double-directional S–V model. Its channel impulse response can be expressed as

$$h(t, \phi_T, \phi_R) = X \sum_{l=0}^{L} \sum_{k=0}^{K} a_{k,l} \delta(t - T_l - \tau_{k,l}) \delta(\phi_T - \phi_{k,l,\mathrm{AoD}}) \delta(\phi_R - \phi_{k,l,\mathrm{AoA}}) \quad (1)$$

where X is the shadowing factor, $a_{k,l}$ the multipath gain coefficient for the kth $(k = 0, \ldots, K)$ ray of the lth $(l = 0, \ldots, L)$ cluster, T_l the arrival time (delay) of the first ray of the lth cluster, $\tau_{k,l}$ the delay of the kth ray of the lth cluster relative to the first ray arrival time T_l, $\phi_{k,l,\mathrm{AoA}}$ and $\phi_{k,l,\mathrm{AoD}}$ the AoA and AoD for corresponding rays, respectively. Since in this paper we only focus on the small scale fading behaviour of the channel, the shadowing factor X will be neglected from this point. Note that by definition, $T_0 = \tau_{0,l} = 0$ [15]. Therefore $\varepsilon_{k,l} = T_l + \tau_{k,l}$ stands for the delay relative to the first arrival and is called 'excess delay'. In this model, the channel impulse response is described as a discrete sum of rays, each characterised by its amplitude, ToA, AoA and AoD. The details of these parameters will be discussed subsequently.

2.2 Angle of arrival and angle of departure

We adopt the approach used in the 3GPP SCM [31] and construct $\phi_{k,l,\mathrm{AoA}}$ and $\phi_{k,l,\mathrm{AoD}}$ from Fig. 1 as

$$\phi_{k,l,\mathrm{AoA}} = \theta_{\mathrm{R}} + \delta_{l,\mathrm{AoA}} + \varphi_{k,l,\mathrm{AoA}} \quad (2)$$

$$\phi_{k,l,\mathrm{AoD}} = \theta_{\mathrm{T}} + \delta_{l,\mathrm{AoD}} + \varphi_{k,l,\mathrm{AoD}} \quad (3)$$

respectively. Here, θ_{R} and θ_{T} are the angles between the transmitter–receiver LOS and the broadside of the transmitter and receiver, respectively, $\delta_{l,\mathrm{AoA}}$ and $\delta_{l,\mathrm{AoD}}$ the AoA and AoD for the lth cluster with respect to θ_{R} and θ_{T}, respectively, $\varphi_{k,l,\mathrm{AoA}}$ and $\varphi_{k,l,\mathrm{AoD}}$ the offset angles for the kth ray

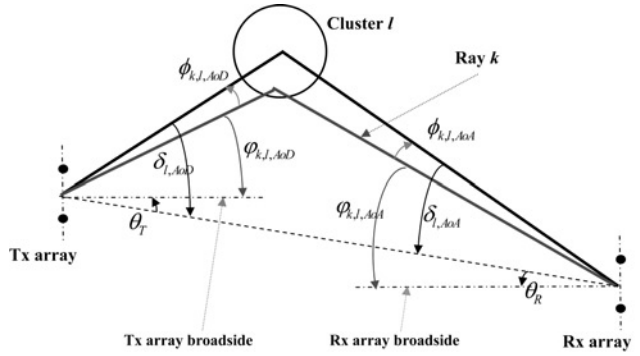

Fig. 1 *Relationships of angles [31]*

of the lth cluster with respect to $\delta_{l,\mathrm{AoA}}$ and $\delta_{l,\mathrm{AoD}}$, respectively.

A few directional measurements of UWB channels are reported in [20, 28, 32–35]. The measured UWB channels are shown to have different directional properties, which likely result from different measurement environments and channel-sounding bandwidth. In this paper, we parameterise the angles in (2) and (3) based on [32, 33]. First, θ_{R} and θ_{T} are treated as independent RVs uniformly distributed from 0 to 360°. Secondly, we assume that $\delta_{l,\mathrm{AoA}}$ and $\delta_{l,\mathrm{AoD}}$ also follow uniform distributions from 0 to 360°. Such a uniform cluster distribution is observed in [32] for non-line-of-sight (NLOS) and in [33] for line-of-sight (LOS) scenarios. Finally, according to measurements in [32], $\varphi_{k,l,\mathrm{AoA}}$ and $\varphi_{k,l,\mathrm{AoD}}$ are Laplacian distributed with zero mean and angle spread $\Omega_{clu} = 38°$. It is assumed that $\phi_{k,l,\mathrm{AoD}}$ and $\phi_{k,l,\mathrm{AoA}}$ are mutually independent and are both independent of the ToA $\varepsilon_{k,l}$. The introduction of correlation into $\phi_{k,l,\mathrm{AoD}}$, $\phi_{k,l,\mathrm{AoA}}$ and $\varepsilon_{k,l}$ is possible but will increase the complexity and reduce the analytical traceability of the channel model.

2.3 Time of arrival

Both T_l and $\tau_{k,l}$ are characterised by Poison processes given by [15]

$$p(T_l|T_{l-1}) = \Lambda \exp[-\Lambda(T_l - T_{l-1})],\ l > 0 \quad (4)$$

$$p(\tau_{k,l}|\tau_{k-1,l}) = \lambda \exp[-\lambda(\tau_{k,l} - \tau_{k-1,l})],\ k > 0 \quad (5)$$

where Λ is the cluster arrival rate and λ the ray arrival rate.

2.4 Amplitudes

In a band-limited, dense multipath channel, an individual resolvable ray is in general the superposition of several irresolvable MPCs, which causes the fading of the ray amplitude $|a_{k,l}|$. Because of the ultra-wide bandwidth of UWB systems, the number of MPCs in a resolvable ray is small, resulting in a much smaller fade depth compared with narrowband systems [1]. Consequently, various amplitude distributions have been suggested [36] to replace the classic Rayleigh distribution, including Nakagami [20, 37], lognormal [38], and Weibull [39, 40] distributions. Following the IEEE 802.15.3a model, we adopt a dual-lognormal distribution that gives the channel amplitude coefficient by [15]

$$a_{k,l} = z_{k,l}\xi_l\beta_{k,l} \quad (6)$$

where $z_{k,l}$ takes the value of equiprobable ± 1 to account for signal inversion because of reflections, ξ_l represents the fading associated with the lth cluster and $\beta_{k,l}$ corresponds to the fading associated with the kth ray of the lth cluster. Both ξ_l and $\beta_{k,l}$ are lognormally distributed RVs given by $\xi_l = 10^{v_l/20}$ and $\beta_{k,l} = 10^{(\mu_{k,l}+v_{k,l})/20}$, respectively. Here, v_l and $v_{k,l}$ are zero-mean Gaussian RVs with standard deviations of a_1 and σ_2, respectively. The mean value $\mu_{k,l}$ is calculated as [15]

$$\mu_{k,l} = \frac{10\ln P_0 - 10T_l/\Gamma - 10\tau_{k,l}/\gamma}{\ln 10} - \frac{(\sigma_1^2 + \sigma_2^2)\ln 10}{20} \quad (7)$$

to fulfil the power delay profile given by [15]

$$E\{|a_{k,l}|^2\} = P_0 \exp\left(\frac{-T_l}{\Gamma}\right)\exp\left(\frac{-\tau_{k,l}}{\gamma}\right) \quad (8)$$

In (7) and (8), Γ is the cluster decay factor, γ the ray decay factor and P_0 the mean energy of the first ray of the first cluster. The values of σ_1 and σ_2 are determined empirically in [15].

3 Correlation-based MIMO-UWB channel construction

3.1 MIMO-UWB channel impulse response and channel matrix

Given an impinging ray that consists of several irresolvable MPCs, different antenna elements at different locations in space might have different perceptions of its amplitude, ToA, AoA and AoD. The differences are related to the propagation environments as well as antenna positions. On the one hand, the amplitude and ToA are in general varied among antenna elements. The amplitude variation is caused by phase-shifted superpositions of irresolvable MPCs, whereas the ToA variation is simply caused by the propagation delays among antenna elements. On the other hand, for small antenna arrays, AoA and AoD appear to be the same for all antenna elements over small spatial variations. From (1), the channel impulse response from the pth ($p = 1, 2, \ldots, n_{\mathrm{T}}$) transmit antenna to the qth ($q = 1, 2, \ldots, n_{\mathrm{R}}$) receive antenna is given by

$$\begin{aligned} h^{p,q}(t, \phi_{\mathrm{T}}, \phi_{\mathrm{R}}) &= \sum_{l=0}^{L}\sum_{k=0}^{K} a_{k,l}^{p,q}\delta(t - T_l^{p,q} - \tau_{k,l}^{p,q}) \\ &\quad \times \delta(\phi_{\mathrm{T}} - \phi_{k,l,\mathrm{AoD}})\delta(\phi_{\mathrm{R}} - \phi_{k,l,\mathrm{AoA}}) \\ &= \sum_{l=0}^{L}\sum_{k=0}^{K} h_{k,l}^{p,q} \end{aligned} \quad (9)$$

where

$$\begin{aligned} h_{k,l}^{p,q} &= a_{k,l}^{p,q}\delta(t - \varepsilon_{k,l}^{p,q})\delta(\phi_{\mathrm{T}} - \phi_{k,l,\mathrm{AoD}}) \\ &\quad \times \delta(\phi_{\mathrm{R}} - \phi_{k,l,\mathrm{AoA}})r \end{aligned} \quad (10)$$

denotes the MPC of the kth ray of the lth cluster from the pth transmit antenna to the qth receive antenna. Note that in (10), $\varepsilon_{k,l}^{p,q} = T_l^{p,q} + \tau_{k,l}^{p,q}$. Let us denote the MIMO channel matrix for the kth ray of the lth cluster as

$$\boldsymbol{H}_{k,l} = \begin{bmatrix} h_{k,l}^{1,1} & \cdots & h_{k,l}^{1,n_{\mathrm{R}}} \\ \vdots & h_{k,l}^{p,q} & \vdots \\ h_{k,l}^{n_{\mathrm{T}},1} & \cdots & h_{k,l}^{n_{\mathrm{T}},n_{\mathrm{R}}} \end{bmatrix} \quad (11)$$

From (10) and (11), $\boldsymbol{H}_{k,l}$ can be expressed by

$$\boldsymbol{H}_{k,l} = \boldsymbol{A}_{k,l} \odot \delta(t - \boldsymbol{\Pi}_{k,l})\delta(\phi_{\mathrm{T}} - \phi_{k,l,\mathrm{AoD}})\delta(\phi_{\mathrm{R}} - \phi_{k,l,\mathrm{AoA}}) \quad (12)$$

where $\odot$ denotes the Hadamard product of matrices. Note

that all calculations in (12) are element-wise operations. The amplitude matrix $\boldsymbol{A}_{k,l}$ and ToA matrix $\boldsymbol{\Pi}_{k,l}$ are defined as

$$\boldsymbol{A}_{k,l} = \begin{bmatrix} a_{k,l}^{1,1} & \cdots & a_{k,l}^{1,n_R} \\ \vdots & a_{k,l}^{p,q} & \vdots \\ a_{k,l}^{n_T,1} & \cdots & a_{k,l}^{n_T,n_R} \end{bmatrix} \quad (13)$$

$$\boldsymbol{\Pi}_{k,l} = \begin{bmatrix} \epsilon_{k,l}^{1,1} & \cdots & \epsilon_{k,l}^{1,n_R} \\ \vdots & \epsilon_{k,l}^{p,q} & \vdots \\ \epsilon_{k,l}^{n_T,1} & \cdots & \epsilon_{k,l}^{n_T,n_R} \end{bmatrix} \quad (14)$$

respectively. The spatial correlation among the entries of $\boldsymbol{A}_{k,l}$ and $\boldsymbol{\Pi}_{k,l}$ will be discussed in the following sections.

3.2 Spatially correlated amplitude matrix $\boldsymbol{A}_{k,l}$

The correlation properties of $\boldsymbol{A}_{k,l}$ are characterised by a $n_T n_R \times n_T n_R$ correlation matrix $\boldsymbol{R}_{k,l}$, whose entry at the $p_1 \times q_1$th row and $p_2 \times q_2$th column ($p_1, p_2 = 1, 2, \ldots, n_T; q_1, q_2 = 1, 2, \ldots, n_R$) is given by the statistical correlation coefficient $\rho_{A,k,l}^{p_1 q_1, p_2 q_2} = \langle a_{k,l}^{p_1,q_1}, a_{k,l}^{p_2,q_2} \rangle$. Here, the subscript A stands for amplitude. Following the idea of a CBSM [19], we can generate spatially correlated amplitude matrix $\boldsymbol{A}_{k,l}$ if $\boldsymbol{R}_{k,l}$ is given or can be calculated. In what follows, we will first describe a procedure of generating correlated $\boldsymbol{A}_{k,l}$ assuming that $\boldsymbol{R}_{k,l}$ is known.

The amplitude coefficient $a_{k,l}$ is given by the product of $z_{k,l}$, ξ_l and $\beta_{k,l}$. The coefficient $z_{k,l}$ because of reflections and the coefficient ξ_l related to cluster fading is similar to the cluster pathloss and can be regarded as constant for all antenna elements over small spatial variations. In contrast, the coefficient $\beta_{k,l}$ related to ray fading will vary among antenna elements because of the superposition of phase-shifted irresolvable MPCs. It follows that

$$a_{k,l}^{p,q} = z_{k,l} \xi_l \beta_{k,l}^{p,q} \quad (15)$$

Consequently, we have $\rho_{A,k,l}^{p_1 q_1, p_2 q_2} = \langle a_{k,l}^{p_1,q_1}, a_{k,l}^{p_2,q_2} \rangle = \langle \beta_{k,l}^{p_1,q_1}, \beta_{k,l}^{p_2,q_2} \rangle$. Note that [15]

$$\beta_{k,l}^{p,q} = 10^{(\mu_{k,l} + v_{k,l}^{p,q})/20} \quad (16)$$

where $\mu_{k,l}$ is calculated from (7) and $v_{k,l}^{p,q}$ are zero-mean Gaussian RVs with identical variances σ_2^2. According to [41], correlated lognormal RVs $\{\beta_{k,l}^{p,q}\}$ can be generated from correlated Gaussian RVs $\{v_{k,l}^{p,q}\}$. The properties of the underlying Gaussian RVs $\{v_{k,l}^{p,q}\}$ are characterised by a $n_T n_R \times n_T n_R$ covariance matrix $\boldsymbol{W}_{k,l}$ whose entires are given by $w_{k,l}^{p_1 q_1, p_2 q_2} = \mathrm{cov}(v_{k,l}^{p_1,q_1}, v_{k,l}^{p_2,q_2})$, where $\mathrm{cov}(\cdot, \cdot)$ denotes the covariance operator. Following similar derivations in [41], we can easily prove that

$$\boldsymbol{W}_{k,l} = (1/\kappa)^2 \ln(1 + e^{(\kappa\sigma_2)^2} \boldsymbol{R}_{k,l}) \quad (17)$$

where κ is a constant given by $\kappa = \ln 10/20$. Note that all calculations in (17) are element-wise operations. Given that $\boldsymbol{W}_{k,l}$ is positive definite, its Choleskey factorisation will produce a colouring matrix $\boldsymbol{C}_{k,l}$, that is, $\boldsymbol{W}_{k,l} = \boldsymbol{C}_{k,l} \boldsymbol{C}_{k,l}^{\mathrm{H}}$, where $(\cdot)^{\mathrm{H}}$ denotes Hermitian transpose. The colouring matrix $\boldsymbol{C}_{k,l}$ can then be used to transform uncorrelated Gaussian RVs to generate $\{v_{k,l}^{p,q}\}$ with desired correlation properties [25], that is

$$\boldsymbol{v}_{k,l} = \boldsymbol{C}_{k,l} \boldsymbol{u}_{k,l} \quad (18)$$

where $\boldsymbol{v}_{k,l}$ is a $n_T n_R \times 1$ column vector given by $\boldsymbol{v}_{k,l} = [v_{k,l}^{1,1}, v_{k,l}^{1,2}, \ldots, v_{k,l}^{1,n_R}, v_{k,l}^{2,1}, \ldots, v_{k,l}^{p,q}, \ldots, v_{k,l}^{n_T,n_R}]^{\mathrm{T}}$ and $\boldsymbol{u}_{k,l}$ is a $n_T n_R \times 1$ column vector whose entries are independent and identically distributed (i.i.d) Gaussian RVs with zero mean and identical variances of 1. Note that $(\cdot)^{\mathrm{T}}$ denotes the transpose operator.

Subsequently, we will discuss how to obtain $\boldsymbol{R}_{k,l}$. In Section 2.2, we constructed the AoA and AoD as mutually independent RVs. This allows us to write the channel correlation coefficients as the product of separable antenna correlations experienced at the transmitter and receiver [25]. This is also known as the Kronecker correlation model. It follows that the amplitude correlation can be calculated by [25]

$$\rho_{A,k,l}^{p_1 q_1, p_2 q_2} = \left| \rho_{C,k,l}^{p_1,p_2} \rho_{C,k,l}^{q_1,q_2} \right|^2 \quad (19)$$

where $\rho_{C,k,l}^{p_1,p_2}$ and $\rho_{C,k,l}^{q_1,q_2}$ are complex antenna correlation coefficients at the transmitter and receiver, respectively. Note that the subscript C stands for complex. According to [42], we can express each resolvable ray as the superposition of M irresolvable random-phase MPCs. It follows that $\rho_{C,k,l}^{p_1,p_2}$ can be calculated as [42]

$$\rho_{C,k,l}^{p_1,p_2} = E\left\{ \frac{1}{M} \sum_{m=1}^{M} \exp\left(j \frac{2\pi c}{f_c} d_{p_1,p_2} \sin(\alpha_{m,k,l,\mathrm{AoD}}) \right) \right\} \quad (20)$$

where c is the speed of light, f_c is the centre frequency, d_{p_1,p_2} is the distance between two transmit antenna elements p_1 and p_2 and $\alpha_{m,k,l,\mathrm{AoD}}$ is the AoD of the mth ($m = 1, 2, \ldots, M$) irresolvable MPC of the kth ray of the lth cluster. The AoD $\alpha_{m,k,l,\mathrm{AoD}}$ is given by

$$\alpha_{m,k,l,\mathrm{AoD}} = \phi_{k,l,\mathrm{AoD}} + \psi_{m,k,l,\mathrm{AoD}} \quad (21)$$

where $\psi_{m,k,l,\mathrm{AoD}}$ is assumed to be uniformly distributed between $[-\Omega, \Omega]$. The parameter Ω characterises the angle dispersion of the irresolvable MPCs. In this paper, we assume that $\Omega = 5^\circ$ and $f_c = 6.85$ GHz.

The number of irresolvable MPCs, M, has an impact on the amplitude fading statistics. For instance, $M \to \infty$ justifies the classic Rayleigh fading. In the case of UWB channels, M is believed to be small, leading to an empirical lognormal fading. In contrast to the impact of M on fading characteristics, we will subsequently show that the amplitude correlation property described by (20) is not affected by M. In Fig. 2, we compare the absolute value of the

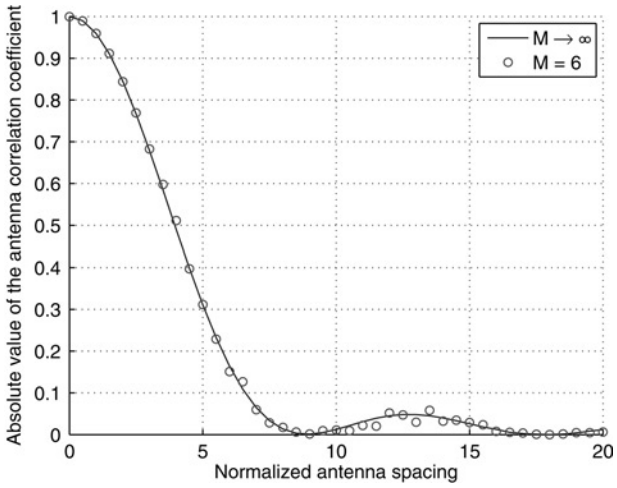

Fig. 2 *Absolute value of transmitter antenna correlation as a function of normalised antenna spacing with different values of $M(\phi_{k,l,AoD} = 50^\circ$, $\Omega = 5^\circ$ and $f_c = 6.85$ GHz)*

transmitter antenna correlation coefficients $|\rho_{C,k,l}^{p_1,p_2}|$ obtained with different values of M. First, with $M \to \infty$, (20) is reduced to [42]

$$\lim_{M\to\infty} \rho_{C,k,l}^{p_1,p_2} = \frac{1}{2\Omega}\int_{\phi_{k,l,\mathrm{AoD}}-\Omega}^{\phi_{k,l,\mathrm{AoD}}+\Omega} \exp\left(j2\pi\frac{f_c}{c} d_{p_1,p_2} \sin\alpha \right) \mathrm{d}\alpha \tag{22}$$

This corresponds to the correlation function of Rayleigh channels and (22) can be calculated numerically [43]. On the other hand, with a small value $M = 6$, (20) is evaluated numerically, where the expectation is taken over $\psi_{m,k,l,\mathrm{AoD}}$ and is computed as the average of 200 realisations. In Fig. 2, we can see that the curve obtained with $M = 6$ is nearly identical with that computed with $M \to \infty$. This is because of the expectation operation in (20), which has similar effects on the antenna correlation to that of increasing M. Based on the above discussion, we propose to use (22) for calculating transmitter antenna correlations of UWB channels. Similarly, the receive antenna correlation $\rho_{C,k,l}^{q_1,q_2}$ can be obtained from $\phi_{k,l,\mathrm{AoA}}$. From (19), it follows that the amplitude correlation coefficient $\rho_{A,k,l}^{p_1q_1,p_2q_2}$ can be obtained. As a typical example, we take the transmit antenna spacing $d_{p_1,p_2} = 10$ cm and receive antenna spacing $d_{q_1,q_2} = 20$ cm, then $|\rho_{A,k,l}^{p_1q_1,p_2q_2}|$ is shown in Fig. 3 as a function of $\phi_{k,l,\mathrm{AoA}}$ and $\phi_{k,l,\mathrm{AoD}}$.

Now, we summarise the four steps of generating spatially correlated $\boldsymbol{A}_{k,l}$: (a) $\boldsymbol{R}_{k,l}$ is computed from (19); (b) $\boldsymbol{W}_{k,l}$ is calculated from $\boldsymbol{R}_{k,l}$ according to (17); (c) correlated Gaussian RVs $\{v_{k,l}^{p,q}\}$ are generated from $\boldsymbol{W}_{k,l}$ based on (18); (d) $\{v_{k,l}^{p,q}\}$ is substituted into (15) and (16) to give correlated $\{a_{k,l}^{p,q}\}$. It is easy to prove that $E\{|a_{k,l}^{p,q}|^2\} = \sigma_{k,l}^2$ regardless of p and q, where $\sigma_{k,l}^2$ denotes the mean energy of the respective ray.

3.3 Spatially correlated ToA matrix $\Pi_{k,l}$

Under the plane wave assumption, an incoming ray has different ToAs among antenna elements because of the propagation delay. We assume uniform linear arrays at both ends and denote the spacing between two adjacent antennas at the transmitter and receiver as d_T and d_R, respectively. The propagation delay for the kth ray of the lth cluster between two adjacent receive antennas is then given by

$$\Delta\epsilon_{k,l}^{\mathrm{Rx}} = \frac{d_\mathrm{R}\sin(\phi_{k,l,\mathrm{AoA}})}{c} \tag{23}$$

where $\phi_{k,l,\mathrm{AoA}}$ is the AoA of the incoming ray and c is the speed of light. Similarly, we have the propagation delay between two adjacent transmitter antennas as

$$\Delta\epsilon_{k,l}^{\mathrm{Tx}} = \frac{d_\mathrm{T}\sin(\phi_{k,l,\mathrm{AoD}})}{c} \tag{24}$$

From the double-directional model, we further assume that for each ray, the ToA difference among the sub-channels is only caused by the propagation delays at transmitter and receiver. Without loss of generality we choose $\epsilon_{k,l}^{1,1}$ as the reference ToA, and it follows that

$$\epsilon_{k,l}^{p,q} = \epsilon_{k,l}^{1,1} + (p-1)\Delta\epsilon_{k,l}^{\mathrm{Tx}} + (q-1)\Delta\epsilon_{k,l}^{\mathrm{Rx}} \tag{25}$$

From (25), the $n_\mathrm{T} \times n_\mathrm{R}$ ToA matrix $\boldsymbol{\Pi}_{k,l}$ with $\epsilon_{k,l}^{p,q}$ as its entries can be written as

$$\boldsymbol{\Pi}_{k,l} = \boldsymbol{\Pi}_{k,l,\mathrm{ref}} + \Delta\boldsymbol{\Pi}_{k,l} \tag{26}$$

where $\boldsymbol{\Pi}_{k,l,\mathrm{ref}}$ is a $n_\mathrm{T} \times n_\mathrm{R}$ reference matrix all of whose entries are $\epsilon_{k,l}^{1,1}$ and $\Delta\boldsymbol{\Pi}_{k,l}$ is a ToA difference matrix given by

$$\Delta\boldsymbol{\Pi}_{k,l} = \begin{bmatrix} 0 & \cdots & (n_\mathrm{R}-1)\Delta\epsilon_{k,l}^{\mathrm{Rx}} \\ \vdots & (p-1)\Delta\epsilon_{k,l}^{\mathrm{Tx}} + (q-1)\Delta\epsilon_{k,l}^{\mathrm{Rx}} & \vdots \\ (n_\mathrm{T}-1)\Delta\epsilon_{k,l}^{\mathrm{Tx}} & \cdots & (n_\mathrm{T}-1)\Delta\epsilon_{k,l}^{\mathrm{Tx}} + (n_\mathrm{R}-1)\Delta\epsilon_{k,l}^{\mathrm{Rx}} \end{bmatrix} \tag{27}$$

Furthermore, we define a $n_\mathrm{T}n_\mathrm{R} \times n_\mathrm{T}n_\mathrm{R}$ ToA domain correlation matrix $\boldsymbol{\Psi}_{k,l}$ whose entries $\Delta\epsilon_{k,l}^{p_1q_1,p_2q_2}$ are given by the ToA difference between two corresponding channels, that is,

$$\begin{aligned}\Delta\epsilon_{k,l}^{p_1q_1,p_2q_2} &= \epsilon_{k,l}^{p_1,q_1} - \epsilon_{k,l}^{p_2,q_2} \\ &= (p_1-p_2)\Delta\epsilon_{k,l}^{\mathrm{Tx}} + (q_1-q_2)\Delta\epsilon_{k,l}^{\mathrm{Rx}}\end{aligned} \tag{28}$$

This matrix $\boldsymbol{\Psi}_{k,l}$ gives an insight into the relationship between antenna spatial positions and the differences of multipath ToAs. Therefore it can be regarded as the equivalent 'correlation matrix' in the ToA domain. As we will show subsequently, this matrix $\boldsymbol{\Psi}_{k,l}$ has a significant impact on the spatial correlation characteristics of the channel.

3.4 Analysis of spatial correlation properties

In this section, we will analyse the spatial correlation properties of the proposed channel model. In particular, we focus on the spatial correlation in the frequency domain, that is, the spatial correlation of channel transfer functions, to provide an insight into frequency-dependent correlation properties of UWB channels. An explicit spatial correlation function will be given, which reveals different impacts of the amplitude correlation matrix $\boldsymbol{R}_{k,l}$ and ToA correlation matrix $\boldsymbol{\Psi}_{k,l}$ on the overall spatial correlation characteristics.

From (9), we can obtain two channel impulse responses $h^{p_1,q_1}(t, \phi_\mathrm{T}, \phi_\mathrm{R})$ and $h^{p_2,q_2}(t, \phi_\mathrm{T}, \phi_\mathrm{R})$, whose complex transfer functions are given by

$$\begin{aligned}H^{p_1,q_1}(f, \phi_\mathrm{T}, \phi_\mathrm{R}) = &\sum_{l=0}^{L}\sum_{k=0}^{K} a_{k,l}^{p_1,q_1} \exp(-j2\pi f \epsilon_{k,l}^{p_1,q_1}) \\ &\times \delta(\phi_\mathrm{T} - \phi_{k,l,\mathrm{AoD}})\delta(\phi_\mathrm{R} - \phi_{k,l,\mathrm{AoA}})\end{aligned} \tag{29}$$

$$\begin{aligned}H^{p_2,q_2}(f, \phi_\mathrm{T}, \phi_\mathrm{R}) = &\sum_{l=0}^{L}\sum_{k=0}^{K} a_{k,l}^{p_2,q_2} \exp(-j2\pi f \epsilon_{k,l}^{p_2,q_2}) \\ &\times \delta(\phi_\mathrm{T} - \phi_{k,l,\mathrm{AoD}})\delta(\phi_\mathrm{R} - \phi_{k,l,\mathrm{AoA}})\end{aligned} \tag{30}$$

respectively. Because of the independent random signal inversion coefficients $z_{k,l}$ described in (15), it is easy to prove that

$$\begin{aligned}E\{a_{k,l}^{p_1,q_1}\} = E\{a_{k,l}^{p_2,q_2}\} &= E\{H^{p_1,q_1}(f, \phi_\mathrm{T}, \phi_\mathrm{R})\} \\ &= E\{H^{p_2,q_2}(f, \phi_\mathrm{T}, \phi_\mathrm{R})\} = 0\end{aligned} \tag{31}$$

Since different rays experience independent fading, their mutual products have zero means. It follows that

$$E\{|H^{p_1,q_1}(f,\phi_T,\phi_R)|^2\} = E\{|H^{p_2,q_2}(f,\phi_T,\phi_R)|^2\} = \sum_{l=0}^{L}\sum_{k=0}^{K} E\{|a_{k,l}^{p,q}|^2\} = \sum_{l=0}^{L}\sum_{k=0}^{K}\sigma_{k,l}^2 \tag{32}$$

From (29)–(32), we can derive the spatial correlation function between $H^{p_1,q_1}(f,\phi_T,\phi_R)$ and $H^{p_2,q_2}(f,\phi_T,\phi_R)$ as

$$\rho_F^{p_1q_1,p_2q_2}(f) = \frac{1}{\sum_{l=0}^{L}\sum_{k=0}^{K}\sigma_{k,l}^2} \times E\left\{\begin{array}{l}\sum_{l=0}^{L}\sum_{k=0}^{K} a_{k,l}^{p_1,q_1} a_{k,l}^{p_2,q_2} \exp(-j2\pi f \Delta\epsilon_{k,l}^{p_1q_1,p_2q_2}) \\ \times\delta(\phi_T-\phi_{k,l,\mathrm{AoD}})\delta(\phi_R-\phi_{k,l,\mathrm{AoA}})\end{array}\right\} \tag{33}$$

Note that in (33), the subscript F of $\rho_F^{p_1q_1,p_2q_2}(f)$ stands for frequency. The expectation operation involves multiple RVs including angular parameters $\phi_{k,l,\mathrm{AoD}}$ and $\phi_{k,l,\mathrm{AoA}}$, as well as lognormal fading amplitudes $a_{k,l}^{p_1,q_1}$ and $a_{k,l}^{p_2,q_2}$. This expectation can be broken down and we can first take expectation over the product $a_{k,l}^{p_1,q_1}a_{k,l}^{p_2,q_2}$ conditioned on $\phi_{k,l,\mathrm{AoA}}$ and $\phi_{k,l,\mathrm{AoD}}$. From (31) and (32), the conditional expectation of $a_{k,l}^{p_1,q_1}a_{k,l}^{p_2,q_2}$ can be related to the amplitude correlation coefficient by

$$E\{a_{k,l}^{p_1,q_1}a_{k,l}^{p_2,q_2}\} = \rho_{A,k,l}^{p_1q_1,p_2q_2}\sqrt{E\{|a_{k,l}^{p_1,q_1}|^2\}}\sqrt{E\{|a_{k,l}^{p_2,q_2}|^2\}} = \sigma_{k,l}^2\rho_{A,k,l}^{p_1q_1,p_2q_2} \tag{34}$$

where $\rho_{A,k,l}^{p_1q_1,p_2q_2}$, as given by (19), is the amplitude correlation coefficient between $a_{k,l}^{p_1,q_1}$ and $a_{k,l}^{p_2,q_2}$ conditioned on $\phi_{k,l,\mathrm{AoA}}$ and $\phi_{k,l,\mathrm{AoD}}$. Substituting (34) into (33), we obtain

$$\rho_F^{p_1q_1,p_2q_2}(f) = \frac{1}{\sum_{l=0}^{L}\sum_{k=0}^{K}\sigma_{k,l}^2} \times E\left\{\begin{array}{l}\sum_{l=0}^{L}\sum_{k=0}^{K} \sigma_{k,l}^2\rho_{A,k,l}^{p_1q_1,p_2q_2} \exp(-j2\pi f \Delta\epsilon_{k,l}^{p_1q_1,p_2q_2}) \\ \times\delta(\phi_T-\phi_{k,l,\mathrm{AoD}})\delta(\phi_R-\phi_{k,l,\mathrm{AoA}})\end{array}\right\} \tag{35}$$

In (35), $\rho_{A,k,l}^{p_1q_1,p_2q_2}$ are entries of the amplitude correlation matrix $\boldsymbol{R}_{k,l}$ and $\Delta\epsilon_{k,l}^{p_1q_1,p_2q_2}$ are entries of the ToA correlation matrix $\Psi_{k,l}$. As described by (19) and (28), both $\rho_{A,k,l}^{p_1q_1,p_2q_2}$ and $\Delta\epsilon_{k,l}^{p_1q_1,p_2q_2}$ are deterministic functions of random angular parameters $\phi_{k,l,\mathrm{AoA}}$ and $\phi_{k,l,\mathrm{AoD}}$. Therefore the expectation in (35) involves merely angular RVs $\phi_{k,l,\mathrm{AoA}}$ and $\phi_{k,l,\mathrm{AoD}}$.

From (35), we can see the impact of amplitude and ToA correlation on the overall spatial correlation function. First, the modelling of ToA correlation is crucial in obtaining frequency dependent properties. Clearly, if we neglect the ToA correlation and force $\Delta\epsilon_{k,l}^{p_1q_1,p_2q_2}=0$, the value of f will be irrelevant since it is multiplied by 0. Secondly, as far as correlation properties are concerned, the modelling of amplitude correlation has a similar effect as spatial filtering. This comes from the fact that the mean power term $\sigma_{k,l}^2$ is multiplied by the amplitude correlation term $\rho_{A,k,l}^{p_1q_1,p_2q_2}$, which is a function of $\phi_{k,l,\mathrm{AoA}}$ and $\phi_{k,l,\mathrm{AoD}}$ as shown previously in Fig. 3. Clearly, MPCs associated with different values of $\phi_{k,l,\mathrm{AoA}}$ and $\phi_{k,l,\mathrm{AoD}}$ will have different attenuations when multiplied by $\rho_{A,k,l}^{p_1q_1,p_2q_2}$, resulting in changes in the effective PAS similar to the effects caused by spatial filters.Third, $\rho_F^{p_1q_1,p_2q_2}(f)$ is sensitive to the PAS in a way that resembles the narrowband spatial correlation analysis [43]. On the other hand, as shown by (35), $\rho_F^{p_1q_1,p_2q_2}(f)$ is not related to the ToA parameters. As a result, we may expect two channels, with distinct ToA characteristics but similar PAS shapes, to have similar correlation patterns. Apart from the above discussions, it is difficult to further simplify (35) analytically. Therefore we will evaluate the properties of the proposed model based on numerical simulations.

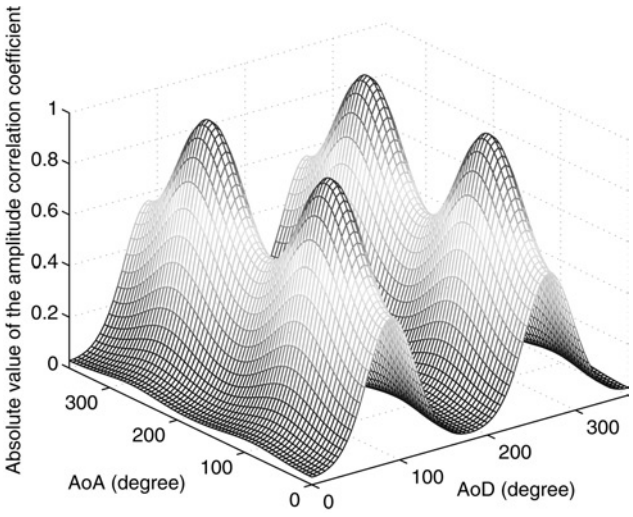

Fig. 3 *Absolute value of amplitude correlation coefficient as a function of AoA and AoD ($d_T = 10$ cm, $d_R = 20$ cm, $\Omega = 5^\circ$ and $f_c = 6.85$ GHz)*

4 Simulation results and discussion

4.1 Realisations of spatially correlated channel impulse responses

The IEEE 802.15.3a UWB channel model (CM) was parameterised to represent four typical scenarios: CM1 for LOS (0–4 m), CM2 for NLOS (0–4 m), CM3 for NLOS (4–10 m) and CM4 for extreme NLOS multipath channels [15]. As an example, we configure our model based on CM2 to simulate an NLOS 2 × 2 MIMO-UWB channel. We assume that $n_T = 2, n_R = 2$, transmitter antenna spacing $d_T = 10$ cm and receiver antenna spacing $d_R = 20$ cm, which are typical configurations of multiple-antenna consumer electronics (e.g. TV, DVD and

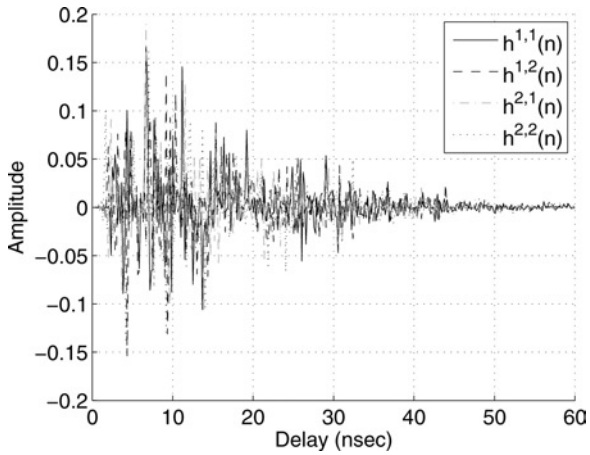

Fig. 4 *Example realisation of four spatially correlated UWB channel impulse responses from the proposed 2 × 2 MIMO-UWB channel model (CM2, $d_T = 10$ cm, $d_R = 20$ cm and $T_s = 0.167$ ns)*

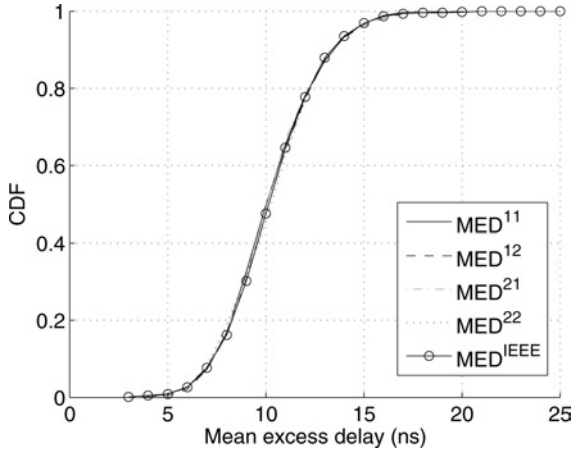

Fig. 5 *The CDFs of mean excess delay of four spatially correlated UWB channels from the proposed 2 × 2 MIMO-UWB channel model and the standard IEEE 802.15.3a UWB model (CM2, $d_T = 10$ cm, $d_R = 20$ cm and $T_s = 0.167$ ns)*

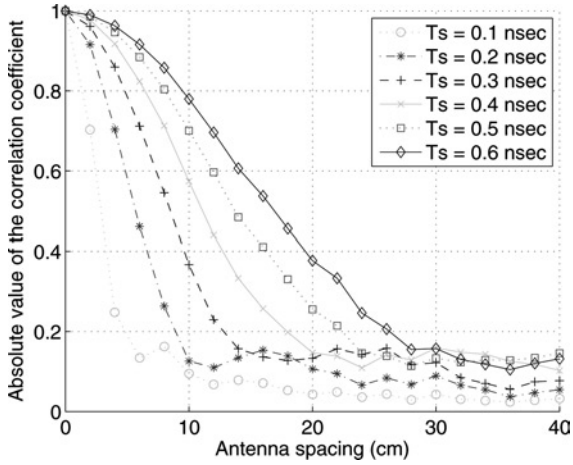

Fig. 6 *Absolute value of the spatial correlation of two channel impulse responses as functions of the antenna spacing d_R and sampling interval T_s*

computer). The amplitude matrices and ToA matrices are generated according to the proposed method. We then discretise each channel impulse response at the sampling interval $T_s = 0.167$ ns according to the procedure specified in [15]. This gives discrete impulse responses for four spatially correlated sub-channels $h^{1,1}(n)$, $h^{1,2}(n)$, $h^{2,1}(n)$ and $h^{2,2}(n)$, where $h^{p,q}(n)$ denotes the discrete channel impulse response between the pth transmit antenna and the qth receive antenna and n is the sample index. An example of realisation of the above four channel impulse responses is shown in Fig. 4.

In theory, the proposed model should be consistent with the IEEE 802.15.3a model. As a validation of our simulation model, we will compare the main channel statistics of the proposed model with those of the IEEE 802.15.3a model. With the proposed model, we generate 1000 random realisations of $h^{1,1}(n)$, $h^{1,2}(n)$, $h^{2,1}(n)$ and $h^{2,2}(n)$. In addition, based on the IEEE 802.15.3a model, 1000 random realisations of a reference SISO channel $h^{\text{IEEE}}(n)$ are generated. For the above five channels, we compare the cumulative distribution functions (CDFs) of their mean excess delay (MED), mean RMS delay, mean number of significant paths capturing more than 85% of the total energy and number of paths within 10 dB of the peak multipath arrival. Their power delay profiles are also compared. Nearly identical curves are observed in all these comparisons. In Fig. 5, we show the comparison regarding the CDFs of MED as an example.

4.2 Spatial correlation of channel impulse responses

We consider a single-input-multiple-output (SIMO) case with one transmit antenna and two receive antennas. The model is configured with CM2, $n_T = 1$ and $n_R = 2$. The receive antenna spacing d_R is set to vary from 0 to 40 cm. For a given d_R, 100 random realisations of discrete channel impulse responses $h^{1,1}(n)$ and $h^{1,2}(n)$ are generated. The correlation characteristics in the time domain can be evaluated by the mean correlation coefficients between $h^{1,1}(n)$ and $h^{1,2}(n)$ given by

$$\hat{\rho}_T(d_R) = E\left\{ \frac{\sum_{n=1}^{N} (h^{1,1}(n) - \bar{h}^{1,1})(h^{1,2}(n) - \bar{h}^{1,2})^*}{\sqrt{\sum_{n=1}^{N} |h^{1,1}(n) - \bar{h}^{1,1}|^2} \times \sqrt{\sum_{n=1}^{N} |h^{1,2}(n) - \bar{h}^{1,2}|^2}} \right\} \quad (36)$$

where $(\cdot)^*$ denotes the conjugate operation, $\bar{h}^{1,1} = 1/N \sum_{n=1}^{N} h^{1,1}(n)$, $\bar{h}^{1,2} = 1/N \sum_{n=1}^{N} h^{1,2}(n)$ and N denotes the total number of samples. The expectation is taken over 100 realisations.

Fig. 6 visualises the absolute value of the correlation coefficient $|\hat{\rho}_T(d_R)|$. We can see that as expected, the correlation decreases with increasing receive antenna spacings. An interesting finding is that a greater T_s leads to a higher correlation. A greater T_s means a lower resolution of the channel, whereas a higher channel correlation in general means reduced diversity, less degrees of freedom and less capacity for a MIMO system. This finding implies that a system with wider bandwidth has greater potential for time-domain multiplexing. The reason for this is that we model the multipath ToA to vary in different sub-channels to take into account the propagation delay. Therefore in the extreme case of infinite resolution ($T_s \to 0$), each multipath is a delta function and the two channel impulse responses are likely to be orthogonal in time. In reality, however, the channel resolution is limited by the system bandwidth and the delay dispersion [17]. Full channel orthogonality in terms of multipath ToAs is unlikely to occur. Nevertheless, wider bandwidth is believed to lower the correlation of channel impulse responses in general. Therefore the multipath and ultra-wide bandwidth nature of a UWB channel could potentially be exploited for spatial multiplexing. This concept was demonstrated in [9] that a higher channel resolution leads to greater multiplexing gains in a Rake decorrelation-based UWB spatial multiplexing system.

4.3 Spatial correlation of channel transfer functions

From the above $h^{1,1}(n)$ and $h^{1,2}(n)$ configured with CM2, the channel transfer functions $H^{1,1}(f)$ and $H^{1,2}(f)$ can be obtained. The correlation properties in the frequency domain are evaluated by

$$\hat{\rho}_F(f, d_R) = \frac{E\{(H^{1,1}(f) - \bar{H}^{1,1}(f)) \times (H^{1,2}(f) - \bar{H}^{1,2}(f))^*\}}{\sqrt{E\{|H^{1,1}(f) - \bar{H}^{1,1}(f)|^2\}} \sqrt{E\{|H^{1,2}(f) - \bar{H}^{1,2}(f)|^2\}}} \quad (37)$$

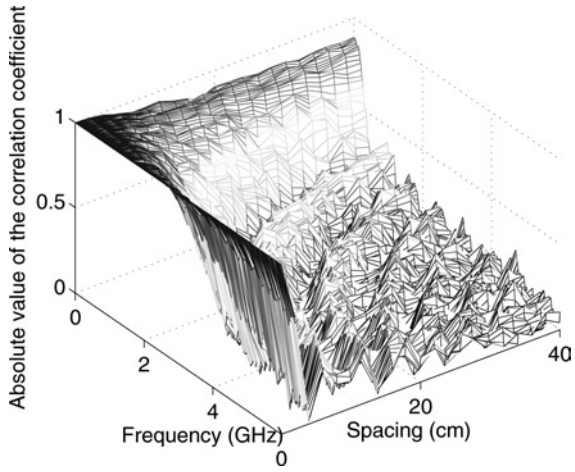

Fig. 7 *Absolute value of the spatial correlation of two channel transfer functions as functions of the frequency f and antenna spacing d_R (CM2, $\Psi_{k,l} \neq 0$ and $T_s = 0.167$ ns)*

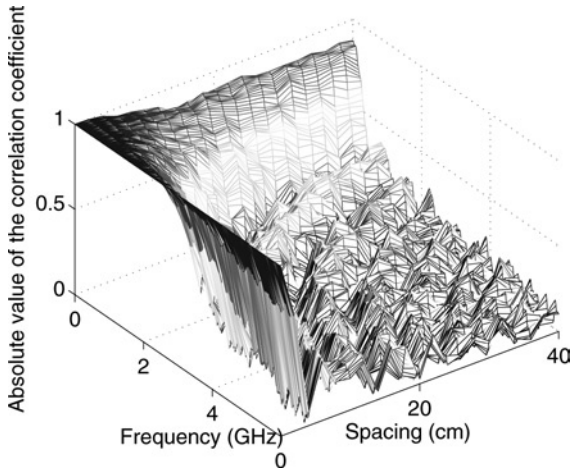

Fig. 9 *Absolute value of the spatial correlation of two channel transfer functions as functions of the frequency f and antenna spacing d_R (CM1, $\Psi_{k,l} \neq 0$ and $T_s = 0.167$ ns)*

where $\bar{H}^{1,1}(f) = E\{H^{1,1}(f)\}$ and $\bar{H}^{1,2}(f) = E\{H^{1,2}(f)\}$. Fig. 7 visualises the absolute value of the correlation coefficient $|\hat{\rho}_F(f, d_R)|$ and three trends are observed. First, at the same frequency band, correlation coefficients decrease with increasing antenna distances. This is similar to narrowband channels where large antenna separation leads to spatially decorrelated channels. Secondly, with the same antenna spacing, higher frequencies result in lower correlation. This agrees with the intuition since two antennas with a certain distance have a different separation in unit of wavelength in different frequency bands. Such an inverse relationship of correlation with frequency in NLOS channels has been experimentally demonstrated in [26, 27]. Thirdly the spatial correlation mainlobe width decreases with the increased frequency, which was confirmed in experiments reported in [27, 28] for NLOS channels.

It is important to mention that the correlation properties shown above largely result from the modelling of the ToA correlation matrix $\Psi_{k,l}$. Fig. 8 shows a case with $\Psi_{k,l} = 0$. We can see that the frequency dependence is lost, which is consistent with the discussion in Section 3-4. Moreover, we can see that the effect of $R_{k,l}$ on $|\hat{\rho}_F(f, d_R)|$ is very limited. This is partially because of the small angular dispersion per ray Ω that we assumed, which leads to relatively high amplitude correlations. From Figs. 7 and 8, we draw the conclusion that $\Psi_{k,l}$, which is proposed as the equivalent correlation matrix in the ToA domain, has a dominant effect on the spatial correlation properties of a multi-antenna UWB channel compared with the amplitude correlation matrix $R_{k,l}$. Therefore we suggest future research on MIMO-UWB channel modelling to be focused on the ToA matrix, in contrast with narrowband or wideband cases.

Since most UWB applications are in LOS environments, it would be interesting to evaluate the model properties in an LOS scenario. Fig. 9 shows the spatial correlation function with CM1 configuration. Comparing Fig. 9 (CM1 based) with Fig. 7 (CM2 based), only marginal difference is observed. The reason is that although CM1 and CM2 differ significantly in ToA statistics, they have similar PAS patterns in our model. As discussed previously in Section 3.4, the spatial correlation function is mostly affected by the PAS and is not relevant to the ToA statistics. In fact, measurements in [27, 29] have also shown that the difference between LOS and NLOS channels in terms of the spatial correlation is indeed not significant.

Finally, Fig. 10 demonstrates the effect of a strong deterministic LOS component on the overall correlation pattern. As an example, we modify the CM1-based channel impulse responses so that the power of the LOS component accounts for one half of the total channel power. Furthermore, the

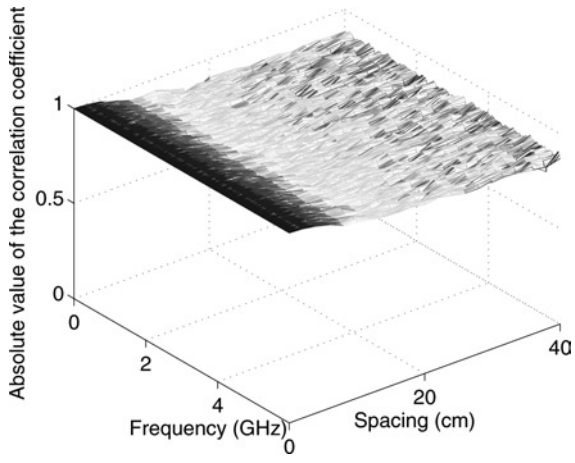

Fig. 8 *Absolute value of the spatial correlation of two channel transfer functions as functions of the frequency f and antenna spacing d_R (CM2, $\Psi_{k,l} = 0$ and $T_s = 0.167$ ns)*

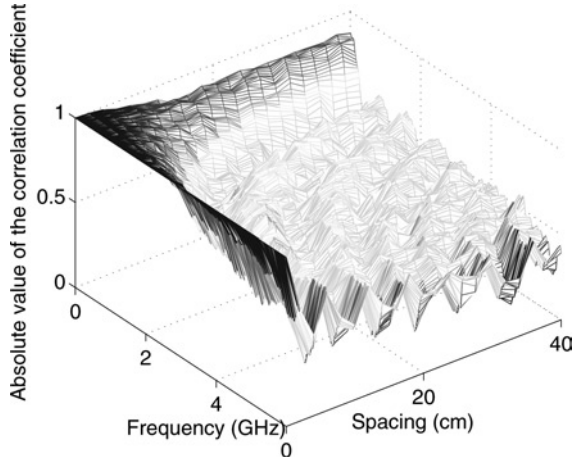

Fig. 10 *Absolute value of the spatial correlation of two channel transfer functions as functions of the frequency f and antenna spacing d_R (Modified CM1 with a strong LOS component, $\Psi_{k,l} \neq 0$ and $T_s = 0.167$ ns)*

AoA and AoD of the deterministic LOS ray are assumed to be $\phi_{0,0,\mathrm{AoD}} = \theta_{\mathrm{T}} = 35^{\circ}$ and $\phi_{0,0,\mathrm{AoA}} = \theta_{\mathrm{R}} = 65^{\circ}$, respectively. Compared with Fig. 9, we can see that the correlation raises significantly. This observation conforms with narrowband experiences that a strong LOS component converts a Rayleigh channel into a Rice channel with increased spatial correlation.

5 Conclusion

In this paper, we have proposed a correlation-based double-directional stochastic model for indoor MIMO-UWB propagation channels. Different from conventional CBSMs, the channel is defined by the real-valued amplitude and ToA of each ray. We propose to introduce spatial correlation to the amplitude matrices and ToA matrices separately. Correspondingly, two correlation matrices are defined explicitly to characterise the correlation properties in both the amplitude and ToA domains. The model is then implemented based on available parameters and evaluated by simulations. We validate our model by first showing it to be consistent with the IEEE 802.15.3a standard model. In addition, simulation-based analysis indicates that the model is able to yield desirable spatial correlation characteristics in both the time and frequency domains. In particular, the correlation frequency dependence, which is typical for MIMO-UWB channels according to various measurement campaigns, is well represented. Finally, the ToA correlation matrices are shown to have a significant impact on the channel correlation pattern, leading to our conclusion that the key to establishing a good analytical channel model for MIMO-UWB systems lies in appropriate modelling of the ToA correlation matrix rather than the amplitude correlation matrix.

6 Acknowledgment

The authors would like to thank Mr. Junsheng Liu at King's College London for helpful discussions.

7 References

1 Allen, B., Dohler, M., Okon, E.E., Malik, W.Q., Brown, A.K., and Edwards, D.J.: 'Ultra-wideband antennas and propagation for communications, radar and imaging' (John Wiley & Sons, West Sussex, England, 2007)
2 Mulvey, D.: 'HSPA', *IET Commun. Eng. Mag.*, 2007, **5**, (1), pp. 38–41
3 Powell, J., and Bannister, D.: 'Business prospects for commercial mm-wave MMICs', *IEEE Microw. Mag.*, 2005, **6**, (4), pp. 34–43
4 Malik, W.Q., Allen, B., and Edwards, D.J.: 'A simple adaptive beamformer for ultrawideband wireless systems'. Proc. IEEE Int. Conf. Ultrawideband (ICUWB), Waltham, MA, USA, September 2006, pp. 453–457
5 Malik, W.Q., and Edwards, D.J.: 'Measured MIMO capacity and diversity gain with spatial and polar arrays in ultrawideband channels', *IEEE Trans. Commun.*, December 2007, **55**, (12)
6 Yang, L.Q., and Giannakis, G.B.: 'Analog space-time coding for multi-antenna ultra-wideband transmissions', *IEEE Trans. Commun.*, 2004, **52**, (3), pp. 507–517
7 Wang, L.C., Liu, W.C., and Shieh, K.J.: 'On the performance of using multiple transmit and receive antennas in pulse-based ultrawideband systems', *IEEE Trans. Wirel. Commun.*, 2005, **4**, (6), pp. 2738–2750
8 Kumar, N.A., and Buehrer, R.M.: 'Application of layered space-time processing to ultra wideband communications'. Proc. 45th Midwest Symp. Circuits and Systems, Tulsa, Oklahoma, August 2002, pp. 597–600
9 Tran, V.P., and Sibille, A.: 'UWB spatial multiplexing by multiple antennas and RAKE decorrelation'. Proc. 2nd Int. Symp. Wireless Communication Systems, Siena, Italy, September 2005, pp. 272–276
10 Zheng, L., and Tse, D.N.C.: 'Diversity and multiplexing: a fundamental tradeoff in multiple antenna channels', *IEEE Trans. Inf. Theory*, 2003, **49**, (5), pp. 1073–1096
11 Chang, T.H., Chang, Y.J., Peng, C.H., Lin, Y.H., and Chi, C.Y.: 'Space time MSINR-SRAKE receiver with finger assignment strategies in UWB multipath channels'. Proc. IEEE Int. Conf. Ultra-Wideband, Zurich, Switzerland, September 2005, pp. 242–247
12 Yang, L.Q., and Giannakis, G.B.: 'Space-time coding for impulse radio'. Proc. IEEE Conf. Ultra Wideband Systems and Technology, Baltimore, MD, USA, May 2002, pp. 235–239
13 Malik, W.Q., and Edwards, D.J.: 'UWB impulse radio with triple-polarization SIMO'. Proc. IEEE Global Communication Conf. (Globecom), Washington, DC, USA, November 2007
14 Keignart, J., Abou-Rjeily, C., Delaveaud, C., and Daniele, N.: 'UWB SIMO channel measurements and simulations', *IEEE Trans. Microw. Theory Tech.*, 2006, **54**, (4), pp. 1812–1819
15 Foerster, J.: Channel Modeling Sub-committee Report Final, IEEE P802. 15-02/368r5-SG3a, 2002
16 Rjeily, C.A., Daniele, N., and Belfiore, J.C.: 'Differential space-time ultra-wideband communications'. Proc. IEEE Int. Conf. Ultra-Wideband, Zurich, Switzerland, September 2005, pp. 248–253
17 Malik, W.Q., and Molish, A.F.: 'Ultrawideband antenna arrays and directional propagation channels'. Proc. Europe Conf. Antennas Propagation (EuCAP), Nice, France, November 2006
18 Shiu, D.S., Foschini, G.J., Gans, M.J., and Kahn, J.M.: 'Fading correlation and its effect on the capacity of multielement antenna systems', *IEEE Trans. Commun.*, 2000, **48**, (3) pp. 502–513
19 Schumacher, L.: 'Recent advances in propagation characterisation and multiple antenna processing in the 3GPP framework'. Proc. XXVIIth URSI General Assembly 2002, Maastricht, The Netherlands, August 2002
20 Kunisch, J., and Pamp, J.: 'Measurement results and modeling aspects for the UWB radio channel'. Proc. IEEE Conf. Ultra Wideband Systems and Technology, Baltimore, MD, USA, May 2002, pp. 19–23
21 Kunisch, J., and Pamp, J.: 'An ultra-wideband space-variant multipath indoor radio channel model'. Proc. IEEE Conf. Ultra Wideband Systems and Technology, Reston, VA, USA, November 2003, pp. 290–294
22 Sibille, A.: 'MIMO diversity for ultra wide band communication', Research report, EURO COST 273 TD(03) 071, 2003
23 Wei, L.Z., Premkumar, B., and Madhukumar, A.S.: 'MMSE detection for high data rate UWB MIMO systems'. Proc. IEEE Vehicular Technology Conf. (VTC), Los Angeles, USA, September 2004, pp. 1463–1467
24 Steinbauer, M., Molisch, A.F., and Bonek, E.: 'The double-directional radio channel', *IEEE Antennas Propag. Mag.*, 2001, **43**, (4), pp. 51–63
25 Kermoal, J.P., Schumacher, L., Pedersen, K.I., and Mogensen, P.E.: 'A stochastic MIMO radio channel model with experimental validation', *IEEE J. Sel. Areas Commun.*, 2002, **20**, (6), pp. 1211–1226
26 Agus, H., Nielsen, J., and Davies, R.J.: 'Correlation analysis for indoor UWB channel'. Proc. Wireless 2005, Calgary, Alberta, Canada, July 2005, pp. 102–110
27 Liu, J., Allen, B., Malik, W.Q., and Edwards, D.J.: 'On the spatial correlation of MB-OFDM ultra wideband transmissions'. Proc. COST 273 Meeting, Bologna, Italy, January 2005
28 Prettie, C., Cheung, D., Rusch, L., and Ho, M.: 'Spatial correlation of UWB signals in a home environment'. Proc. IEEE Conf. Ultra Wideband Systems and Technology, Baltimore, MD, USA, May 2002, pp. 65–69
29 Liu, J., Allen, B., Malik, W.Q., and Edwards, D.J.: 'A measurement based spatial correlation analysis for MB-OFDM ultra wideband transmissions'. Proc. Loughborough Antennas Propagation Conf. (LAPC), Loughborough, UK, April 2005
30 Saleh, A., and Valenzuela, R.A.: 'A statistical model for indoor multipath propagation', *IEEE J. Sel. Areas Commun.*, 1987, **5**, (2), pp. 137–138
31 3GPP, TR 25.996: 'Spatial channel model for multiple input multiple output (MIMO) simulations (Rel. 6)' 2003
32 Cramer, R.J.M., Scholtz, R.A., and Win, M.Z.: 'Evaluation of an ultra-wide-band propagation channel', *IEEE Trans. Antennas Propag.*, 2002, **50**, (5), pp. 561–570
33 Haneda, K., Takada, J., and Kobayashi, T.: 'Double directional ultra wideband channel characterization in a line-of-sight home environment', *IEICE Trans. Fundam.*, 2005, **E88-A**, (9), pp. 2264–2271
34 Cramer, J.M., Scholtz, R.A., and Win, M.Z.: 'Spatio-temporal diversity in ultra-wideband radio'. Proc. IEEE Wireless Communication and Network Conf. (WCNC), 1999, vol. 2, pp. 888–892
35 Karedal, J., Wyne, S., Almers, P., Tufvesson, F., and Molish, A.F.: 'Statistical analysis of the UWB channel in an industrial

environment'. Proc. IEEE Vehicular Technology Conf. (VTC), Los Angeles, USA, September 2004, pp. 81–85
36 Molish, A.F.: 'Ultrawideband propagation channels-theory, measurement, and modeling', *IEEE Trans. Veh. Technol.*, 2005, **54**, pp. 1528–1545
37 Cassioli, D., Win, M.Z., and Molisch, A.F.: 'The ultra-wide bandwidth indoor channel: from statistical model to simulations', *IEEE J. Sel. Areas Commun.*, 2002, **20**, (6), pp. 213–217
38 Foerster, J.R., and Li, Q.: 'UWB channel modeling contribution from intel', IEEE Technical Report P802.15 02/279SG3a, 2002
39 Alvarez, A., Valera, G., Lobeira, M., Torres, R., and Garcia, J.L.: 'New channel impulse response model for UWB indoor system simulations'. Proc. Vehicular Technology Conf. (VTC) Spring, 2003, pp. 1–5
40 Pagani, P., and Pajusco, P.: 'Experimental assessment of the UWB channel variability in a dynamic indoor environment'. Proc IEEE PIMRC, 2004, pp. 2973–2977
41 Peebles, P.Z.: 'The generation of correlated log-normal clutter for radar simulations', *IEEE Trans. Aerosp. Electron. Syst.*, 1971, **AES-7**, (6), pp. 1215–1217
42 Wang, C.X., Hong, X., Wu, H., and Xu, W.: 'Spatial temporal correlation properties of the 3GPP spatial channel model and the Kronecker MIMO channel model', *EURASIP J. Wirel. Commun. Netw.*, Vol. 2007, Article ID 39871, 9 pages, 2007, doi: 10.1155/2007/39871
43 Schumacher, L., Pedersen, K.I., and Mogensen, P.E.: 'From antenna spacings to theoretical capacities - guidelines for simulating MIMO systems'. Proc. 13th IEEE Int. Symp. Personal, Indoor & Mobile Radio Communication (PIMRC), Lisboa, Portugal, September 2002, pp. 587–592